Estimation of stresses in atmospheric ice during aeolian vibration of power transmission lines

Majid Kermani, Masoud Farzaneh and László E. Kollár

NSERC/Hydro-Québec/UQAC Industrial Chair on Atmospheric Icing of Power Network Equipment (CIGELE), and Canada Research Chair on Atmospheric Icing Engineering of Power Networks (INGIVRE), Université du Québec à Chicoutimi, Chicoutimi, Qué., Canada G7H 2B1 (www.cigele.ca)

Abstract

Aeolian vibration in bare and iced cable was simulated using the theory of cable vibration. High frequency vibration creates stresses in the cable and consequently in the ice covering that cable, which may result in ice failure and eventually ice shedding. These stresses were estimated in this study. Displacement of the cable during vibration was determined; furthermore, instantaneous wind loads in vertical and transverse directions, additional stresses induced by the motion in the cable and in the atmospheric ice, as well as torque due to cable springback were calculated. In order to simulate the loading conditions of a chunk of atmospheric ice in the middle of a span, a new model was developed using ABAQUS. Results from this model show in spite of high frequency vibration, the resulting level of stress in atmospheric ice is far less than its failure limit. In other words, the atmospheric ice under the condition assumed in this investigation does not shed due to aeolian vibration.

Keywords: Atmospheric ice, cable, aeolian vibration, model, stress

GLOSSARY OF NOTATIONS

A_c	Cross section area of the cable
A_i	Cross section area of the atmospheric ice
C	Damping coefficient per unit length
C_D	Drag coefficient
C_1	Material constant
C_L	Lift coefficient
d	Sag of the cable
d_c	Cylinder diameter
D_i	Diameter of atmospheric ice
$\mathrm{d}s$	Cable segment
$\mathrm{d}s'$	Deformed cable segment
E_c	Young's modulus of the cable
E_i	Young's modulus of the atmospheric ice
F_0	Cable excitation amplitude
f_v	Vortex shedding frequency
GJ	Torsional rigidity of the cable
H	Horizontal component of the cable tension
$h(t)$	Additional horizontal component of cable tension as a function of time
$\tilde{h}$	Constant
L	Span length
L_1	Length of a piece of cable in the middle of the span
L_c	Cable length
m	Mass per unit length of the cable including the ice mass
p	Wind power
s	Spatial coordinate along the curved length of the cable
S_s	Strouhal number
t	Time
T_0	Static tension of the cable
T_a	Additional dynamic tension in the cable

T_A	Torque at the suspension points of the cable
T_c	Torque due to springback of the cable
$U(s, t)$	Cable displacement in the horizontal direction
U_o	Velocity of wind or flow
$V(s, t)$	Cable displacement in the vertical direction
$W(s, t)$	Cable displacement in the transverse direction
x	Coordinate along the cable span
y	Amplitude of the vibration
$y(s)$	Static profile of the cable
θ	Cable rotation at mid-span around its centerline
ω_s	Frequency of aeolian vibration
ξ	Damping ratio in vertical direction
$\varphi_i(s)$	Mode shape in the vertical direction
ρ_a	Air density
ν_{air}	Kinematic viscosity of air.

1. Introduction

Power transmission lines are vulnerable to winds and storms, particularly in cold climate regions where atmospheric ice accretes on network equipment. The interaction of natural wind with the surface roughness of the earth produces a wind character that is gusty or turbulent as opposed to being smooth and uniform. Wind turbulence or gusts produce velocity fluctuations that are spatial and temporal in character. Therefore, the wind force acting on a cable will vary in direction as well as in magnitude vertically and horizontally at any point in time. When ice or wet snow accretion builds up on conductors of overhead power lines, and a wind force acts across the resulting profile, the conductors can rotate and move with low amplitude high frequency vibration (aeolian vibration), with high amplitude

low frequency vibration (galloping), or with vibration of amplitude and frequency in between (wake-induced oscillation). However, this latter type of vibration is peculiar to bundled conductors only. The primary cause of aeolian vibration is the alternate shedding of wind-induced vortices from the top and bottom sides of the conductor. This action creates an alternating pressure imbalance, inducing the conductor to move up and down at right angles to the direction of airflow.

When the cable is covered with ice, stresses develop both in the cable and in the ice. The stresses developing in the ice during galloping were studied in [9]; whereas the purpose of the present paper is to estimate those stresses during aeolian vibration.

2. Aeolian vibration in power transmission lines

The three primary variables involved in vortex shedding from a circular cylinder are the cylinder diameter, the fluid velocity, and the kinematic viscosity of the particular fluid. The wind power, p, transferred from the wind to a vibrating conductor may be expressed in the following general form:

$$p = d_c^{\,4} f_v^{\,3} fnc\left(\frac{y}{d_c}\right) \qquad (1)$$

where d_c is the outside diameter of the bare or iced cable, f_v is the vortex shedding frequency in units of Hz, and y is the vibration amplitude [2].

The vibration amplitude is determined by a power balance between what is provided by the wind and what is dissipated by the cable self-damping and by any dampers. Ice and/or snow precipitations affect aoelian vibration through different mechanisms. A snow cover may smooth terrain obstacles that would normally contribute to wind velocity fluctuations. A more closely constant wind velocity and azimuth will give results that are more propitious to severe aeolian vibration [13].

When ice is present, other factors will also contribute to increasing the severity of aeolian vibration. For example, an iced conductor may lock cable strands together so that cable internal damping through strand slippage decreases. Moreover, it is well known that internal cable damping depends heavily on the cable's mechanical tension. The ice weight will increase cable tension, which will also reduce conductor self-damping.

Eq. 1 shows that when ice accretion increases, assuming the cable diameter and frequency remains constant, aeolian power increases to about the fourth power of the outside diameter of the iced cable [5].

Aeolian vibration has been studied by other researchers (e.g. [3, 4]). To the authors' knowledge, however, a comprehensive analysis for determining the displacement of each point of the cable with accreted ice in aeolian vibration that covers the damping effect and wind force has never previously been published.

In order to simulate aeolian vibration and estimate the stresses in atmospheric ice during that vibration, it is necessary to model the cable motion and obtain the position of each point along the cable. Therefore, the equation of motion describing cable vibration should be studied. For a more accurate estimation, the following forces and stresses should be applied onto atmospheric ice: aerodynamic forces, additional tension in cable due to vibration, ice mass inertia and torque due to cable springback.

Owing to the complexity of this problem, some sophisticated aspects of the natural conditions must be simplified, as follows:

a) Normally, ice shapes on power transmission lines are not exactly cylindrical and uniform; it is more closely symmetrical in the middle of the span than in other parts. Still, cylindrical and uniform ice shape is assumed all along the cable. However, in the calculation of wind

loads on the cable, the wind force functions obtained from wind tunnel tests for asymmetrically iced cables are used.

b) Movements and vibration of towers during cable vibration are assumed to be negligible.

c) Wind velocity is assumed to be constant during aeolian vibration, and uniform all along the cable.

2.1 Equation of motion in aeolian vibration

The basic equations of motion of a suspended cable are the following [1, 6, 10, 11].

$$\frac{\partial}{\partial s}[(T_0+T_a)\frac{\partial(x+U)}{\partial s}]=m\frac{\partial^2 U}{\partial t^2} \tag{2}$$

$$\frac{\partial}{\partial s}[(T_0+T_a)\frac{\partial(y+V)}{\partial s}]=-mg+m\frac{\partial^2 V}{\partial t^2}+c\frac{\partial V}{\partial t}+F_1(s,t) \tag{3}$$

$$\frac{\partial}{\partial s}[(T_0+T_a)\frac{\partial W}{\partial s}]=m\frac{\partial^2 W}{\partial t^2}+c\frac{\partial W}{\partial t}+F_2(s,t) \tag{4}$$

where s is the spatial coordinate along the curved length of the cable; t is the time; x is the coordinate along the cable span; $y(s)$ is the cable static profile; $U(s, t)$, $V(s, t)$ and $W(s, t)$ are, respectively, the displacement in the horizontal, vertical and transverse directions (Fig.1), m is the cable mass per unit length, including ice mass, c is the damping coefficient per unit length, T_0 is the static tension; T_a is the additional dynamic tension in the cable; $F_1(s, t)$, and $F_2(s, t)$ are, respectively, the external loading per unit length in the vertical and transverse directions. When additional dynamic tension is applied to the cable with accreted ice, this tension is divided between the cable and ice according to the following relations:

$$T_{ac}=\frac{T_a A_c E_c}{A_c E_c+A_i E_i} \tag{5}$$

$$T_{ai}=\frac{T_a A_i E_i}{A_c E_c+A_i E_i} \tag{6}$$

where E_i and E_c are Young's modulus of atmospheric ice and cable, and A_i and A_c are cross section areas of the ice and cable, respectively. Since the ratio of sag to span in power transmission lines is less than 1:8 and horizontal loads are negligible in our model, we can consider the horizontal displacement U to be equal to zero [1, 6, 10].

As mentioned before, the conductor motion during aeolian vibration occurs only in vertical direction whereupon the displacement in transverse direction W will be zero as well. Then, Equation (3) can be written for aeolian vibration as below [6]:

$$HV''(x,t) + h(t)\left(\frac{-8d}{L^2}\right) = m\ddot{V}(x,t) + c\dot{V}(x,t) + F_0 \sin(\omega_s t) \tag{7}$$

where $h(t)$ is defined as the additional horizontal component of cable tension induced by the motion and is a function of time alone, and H denotes the horizontal component of cable tension which can be obtained by solving (8) numerically:

$$d = \frac{H}{mg}[\cosh(\frac{mgL}{2H}) - 1] \tag{8}$$

where d is the sag of the cable and L is span length. The last two terms in the right-hand side of Eq. (7) account for cable damping and the excitation due to wind. The amplitude of the excitation force per unit length, F_0, and circular frequency, ω_s, of this excitation are determined as follows:

$$F_0 = \frac{1}{2}\rho_a C_L D_i U_0^2 \tag{9}$$

$$\omega_s = 2\pi \frac{S_s U_0}{D_i} \tag{10}$$

respectively, where ρ_a is air density , C_L is the lift coefficient, D_i is the diameter of iced cable, U_0 is air velocity, S_s is Strouhal number, and the circular frequency, ω_s, obtained this way is the circular vortex shedding frequency.

Eq. (7) is solved by assuming that

$$V(x,t)=\sum_i \varphi_i(x)T_i(t) \tag{11}$$

and

$$h(t)=\sum_i \tilde{h}_i T_i(t) \tag{12}$$

where $\varphi_i(x)$ is obtained by using the linear theory of cable vibration [6]:

$$\varphi_i(x)=\frac{8d\tilde{h}}{H(\beta_i L)^2}\left(1-\tan\left(\frac{1}{2}\beta_i L\right)\sin(\beta_i x)-\cos(\beta_i x)\right) \tag{13}$$

and

$$\beta_i=\omega_{v,i}\sqrt{\frac{m}{H}} \tag{14}$$

with $\omega_{v,i}$ denoting the natural frequency in the vertical direction.

The parameter β_i can be calculated from the following equation [6]:

$$\tan\left(\frac{1}{2}\beta L\right)=\left(\frac{1}{2}\beta L\right)-\left(\frac{4}{\lambda^2}\right)\left(\frac{1}{2}\beta L\right)^3 \tag{15}$$

where λ^2 takes the form:

$$\lambda^2=\left(\frac{8d}{L}\right)^2\frac{L}{(HL_e/E_cA_c)} \tag{16}$$

$$L_e=\int_0^L\left(\frac{ds}{dx}\right)^3 dx\approx L\left(1+8\frac{d^2}{L^2}\right) \tag{17}$$

Substituting (11) and (12) into (7) gives:

$$\sum_i H\varphi_i''T_i-\sum_i\frac{8d}{L^2}\tilde{h}_iT_i=\sum_i m\varphi_i\ddot{T}_i+\sum_i c_i\varphi_i\dot{T}_i+F_0\sin(\omega_s t) \tag{18}$$

According to [6], $\varphi_i(x)$ is a solution of

$$HV''(x,t)+h(t)\left(\frac{-8d}{L^2}\right)=m\ddot{V}(x,t) \tag{19}$$

with Eqs. (11) and (12). Then, the equation for the *i*th vibration mode takes the form

$$H\varphi_i''T_i-\frac{8d}{L^2}\tilde{h}_iT_i=m\varphi_i\ddot{T}_i \tag{20}$$

where $T_i(t)$ is defined as follows:

$$T_i(t) = \mathrm{e}^{j\omega_i t} \tag{21}$$

Substituting (21) into (20) gives

$$H\varphi_i''\mathrm{e}^{j\omega_i t}=-m\varphi_i\omega_i^2\mathrm{e}^{j\omega_i t}+\frac{8d}{L^2}\tilde{h}_i\mathrm{e}^{j\omega_i t} \tag{22}$$

Dividing (22) by $\mathrm{e}^{j\omega_i t}$ and substituting it into (18) we obtain:

$$-\sum_i m\varphi_i\omega_i^2T_i=\sum_i m\varphi_i\ddot{T}_i+\sum_i c_i\varphi_i\dot{T}_i+F_0\sin(\omega_s t) \tag{23}$$

Multiplying each term by $\varphi_n(x)$ and integrating gives:

$$-\sum_i m\omega_i^2T_i\int_0^L\varphi_i\varphi_n dx=\sum_i m\ddot{T}_i\int_0^L\varphi_i\,\varphi_n dx+\sum_i c_i\dot{T}_i\int_0^L\varphi_i\varphi_n dx+F_0\sin(\omega_s t)\int_0^L\varphi_n dx \tag{24}$$

Applying the orthogonality conditions:

$$\int_0^L\varphi_m\varphi_n''dx=0 \qquad \text{if } m\neq n \tag{25}$$

we obtain

$$-m\omega_n^2T_n\int_0^L\varphi_n^2dx=m\ddot{T}_n\int_0^L\varphi_n^2dx+\sum_i c_n\dot{T}_n\int_0^L\varphi_n^2dx+F_0\sin(\omega_s t)\int_0^L\varphi_n dx \tag{26}$$

Equation (26) can be rewritten as below

$$m\ddot{T}_n+c_n\dot{T}_n+m\omega_n^2T_n=-F_0\sin(\omega_s t)\frac{\int_0^L\varphi_n dx}{\int_0^L\varphi_n^2dx} \tag{27}$$

where

$$c_n=2m\omega_n\zeta_n \tag{28}$$

with ζ_n standing for structural damping factor [2]. Equation (27) depends only on time, and its general solution is the sum of the homogeneous, T_h, and particular, T_p, solutions:

$$T_n=T_h+T_p \tag{29}$$

The homogeneous solution of this differential equation is obtained by solving the characteristic equation:

$$mr^2 + c_n r + m\omega_n^2 = 0 \tag{30}$$

where r is the characteristic root:

$$r_{1,2} = \frac{-c_n \pm \sqrt{{c_n}^2 - 4m^2\omega_n^2}}{2m} = \frac{-2m\omega_n\zeta_n \pm \sqrt{4m^2\omega_n^2({\zeta_n}^2 - 1)}}{2m} = -\omega_n\zeta_n \pm j\omega_n\sqrt{1-\zeta_n^2} \tag{31}$$

Therefore, the homogeneous solution is

$$T_h = A_n e^{-\omega_n\zeta_n t}\cos(\omega_n t\sqrt{1-\zeta_n^2}) + B_n e^{-\omega_n\zeta_n t}\sin(\omega_n t\sqrt{1-\zeta_n^2}) \tag{32}$$

The particular solution of Equation (27) is obtained by substituting

$$T_p = p_n\cos\omega_s t + q_n\sin\omega_s t \tag{33}$$

into Equation (27). After determining the constants p_n and q_n, the particular solution is expressed in the form

$$T_p = \frac{F_0}{c\omega_s}\frac{\int_0^L \varphi_n dx}{\int_0^L \varphi_n^2 dx}\cos(\omega_s t) \tag{34}$$

Since aeolian vibration in steady state is modeled here, and $T_h \to 0$ when $t \to \infty$, the vertical displacement, $V_n(x,t)$, may be written as a product of $\varphi_n(x)$ given by Equation (13) for $i = n$ and $T_p(t)$ given by Equation (34). This expression provides the displacements of each point along the cable in vertical direction that will be calculated and tabulated by a MATLAB code.

2.2 Loads and stresses in atmospheric ice during aeolian vibration

- **Stresses due to cable vibration**

A dynamic load acting from ice during aeolian vibration is induced by acceleration due to cable motion or gravity force. This vibration also creates some elastic deformation in the cable that induces more stresses in the atmospheric ice. The effect of these loads is calculated in this model by means of the ABAQUS software. The position of each point along the cable during aeolian vibration (calculation results are presented in Section 2.1) will be used as input in the ABAQUS model to determine the stresses developing in the atmospheric ice.

• Aerodynamic forces

As mentioned above, aerodynamic forces cause cable vibration and this movement can produce some stresses and additional tension in the cable. However, these forces also apply some loads directly on the atmospheric ice which are expressed by the following equations [2]:

$$F_v = F_0 \sin(\omega_s t) \tag{35}$$

$$F_w = \frac{1}{2}\rho C_D D_i U_0^2 \tag{36}$$

where C_D is the drag coefficient. To take into account the effect of these forces on a piece of atmospheric ice in the middle of a span, it is sufficient to apply them in the ABAQUS model as a distributed force on the ice (see Fig. 2).

• Torsional loads

Power transmission cables are very flexible and tend to rotate when ice builds up asymmetrically on their surface. As mentioned in [9], the relationship between the rotation of the cable at mid-span around its centerline, θ, and the torque at the suspension points, T_A, due to cable springback can be written as follows :

$$\frac{T_A \frac{L_c}{2}}{GJ} = \theta \tag{37}$$

where GJ is the torsional rigidity of cable, L_c is the cable length, and where constant ice thickness is assumed along the entire span. Once θ is known, the torque of springback ,T_c, which is applied by the cable to the end point of a piece of ice located in the middle of the span, can be determined as follows:

$$T_C = \frac{2\theta L_1 GJ}{L_c{}^2} \tag{38}$$

where L_1 is the length of the piece of cable (torque in Fig. 2). Since a short piece of the cable-ice composition in the middle of the span is analyzed, i.e. $L_1 << L_c$, the torque, $T_{C,}$ is significantly smaller than the other loads discussed above.

• **Additional dynamic tension in the cable and the ice**

As mentioned above, cable motion during aeolian vibration induces additional tension in the cable and atmospheric ice. The stresses due to these additional tensions are calculated using the following formulae:

$$\sigma_c = E_c \frac{ds' - ds}{ds} \tag{39}$$

$$\sigma_i = E_i \frac{ds' - ds}{ds} \tag{40}$$

where ds' is the deformed cable segment. These terms were considered in the model constructed with ABAQUS (additional tensions in Fig. 2).

Also, the stresses due to ice load and ice mass inertia will be taken into account in the ABAQUS model.

The results of all calculations are eventually used in a model constructed using the ABAQUS finite element software. This model provides an estimation of stress level in different parts of the ice on the cable and its variation during aeolian vibration.

2.3 Calculation of forces and displacements

The cable motion during aeolian vibration is simulated by a program developed with MATLAB. The cable and ice characteristics, the wind velocity, U_0, and the damping ratio in the vertical direction, ζ, are defined as input data for the MATLAB implementation. This program determines the displacements of two ends of a piece of cable with ice in the middle of the span. Furthermore, it computes the aerodynamic forces on the ice, the torque applied to the ice due to cable springback, and the additional tension induced by the motion in the cable and the ice. All of these values are tabulated as time functions, and then are used as loads and displacements in the ABAQUS model described in the next section.

3. Modeling stress variation during aeolian vibration with ABAQUS

The simulation of cable motion and the load calculation provide all the parameters needed to determine the stress in the ice and its variation during aeolian vibration. A model of a piece of cable with uniform cylindrical ice accretion is constructed in ABAQUS, which computes the stress developing in the ice through one or more cycles of aeolian vibration. The curves representing cable motion at each end of the modeled piece, as sketched in Fig. 2, are obtained as output data of the MATLAB program. The additional cable tension and aerodynamic forces are also added as input data, while the effect of ice load and inertia is determined in the ABAQUS calculation.

The analysis was carried out in Dynamic Explicit condition with ABAQUS, which uses a consistent, large-deformation theory, so that the model can undergo large rotations and large

deformation. The element type for cable and ice is C3D8R. This is a three-dimensional element with 8 nodes and suitable for continuum stress/displacement analysis with reduced integration. The variations of vertical displacement, aerodynamic forces, additional tension in the cable and the ice were tabulated in 6 tables. Each table has two columns, the first one containing the time data, while the second one lists the above-mentioned parameters at each instance. The total time of analysis is 0.3 s. In order to have more accurate estimation, both ends of the cable-ice piece at the beginning of the analysis were set in the positions which represent the initial shape of the ice and cable before any deformation. The ice was assumed to adhere strongly to the cable surface without sliding and separation.

4. Results and discussion

The preliminary calculations with MATLAB and the stress analysis in ABAQUS were applied for a typical example. Table 1 shows the characteristics of the span, cable and ice considered in this example. The value of rotation angle due to ice accretion at span centre has been obtained from simulation of atmospheric ice accretion conducted by Fu [8].

According to the results of the MATLAB code, the amplitude of aeolian vibration for the BERSIMIS cable with a thickness of 2.5 cm accreted ice in a wind of 4 m/s velocity is 58.1 mm. EPRI [5] reported that the amplitude of aeolian vibration in field measurements varied in the range of 0.01 and 1 cable diameter. Considering the ice load on the cable, the corresponding interval occurs between 0.85 mm and 85 mm in the specific example of this study, so that the value of vibration amplitude calculated by MATLAB code falls in that range.

The cable displacement in the middle of the span in vertical direction is shown in Fig. 3. A full cycle of aeolian vibration lasts 0.12 s. The results of wind load and stress calculations are

presented in Figs. 4 and 5. Fig. 4 shows the variation of the distributed wind force in vertical direction during a full cycle of vibration, whereas Fig. 5 shows the stresses due to additional dynamic tension in the cable and atmospheric ice.

The data presented in Table 1 and the results of the calculations discussed in Sections 2.1 and 2.2 were applied as inputs for the stress analysis on a 10-cm piece of the cable-ice composite in the middle of the span. The results of the calculated Von Mises stresses in several elements during a 0.3-second interval of aeolian vibration in various positions are shown in Figs. 6 and 7. The positions of these elements in the middle of the 10-cm piece of the ice cover are illustrated in Fig. 8. Figs. 6 and 7 show that the Von Mises stresses reach their maximum values when the mid-point of the cable is at the highest and lowest positions of its trajectory. Numerically, these maximum values are 6210 Pa for the elements in the external layer, and 4056 Pa for the elements in the internal layer.

The bending strength of atmospheric ice was measured in a parallel research whose results were published in [7]. Those observations ascertained that the bending strength of atmospheric ice at -10 ^{o}C varied with strain rate. According to the guidelines recommended by the IAHR (International Association of Hydraulic Engineering and Research) working group on test methods [12], experiments with loading times to failure on the order of 1 second yield satisfactory results for bending strength of ice. In [7] this load rate corresponds to the strain rate of 2×10^{-3} s^{-1} yielding a value of approximately 2.73 MPa for bending strength of atmospheric ice, which gives a reasonable value for tensile strength and can be used here as failure limit of atmospheric ice.

Figs. 9 and 10 show normal stresses in vertical direction (perpendicular to the cable axis) in the same elements as in Figs. 6 and 7, respectively. When the cable approaches its highest

position, the elements on the top of the cable (elements No. 435 and 433) are under tension, whereas the bottom elements (No. 8 and 200) are under compression. The stress direction changes when the cable approaches its lowest position. The elements close to the neutral axis (elements No. 904, 280, 88 and 448) endure less stress because the strains are smaller in that area.

Figs. 11 and 12 show the distribution of Von Mises stresses along the horizontal and vertical diameters of the iced cable in the middle of the 10-cm piece at 0.17s. As expected and observed in the case of galloping [9], the stresses in the internal layers of the ice (and cable) are less than in the external layers. Comparing the stress level in atmospheric ice during aeolian vibration and the bending strength of atmospheric ice, it was observed that under the conditions of this study, the stresses developing during aeolian vibration were not great enough to cause ice failure. The simulation results in [9] showed that ice failed during galloping for a minimum wind speed of 4.5 – 5.2 m/s, which caused vibration with amplitude between 1.65 m and 2.45m. Since the vibration amplitude, and consequently, the stress in the ice are at least one order of magnitude lower than during galloping, ice failure during aeolian vibration may occur due to fatigue rather than due to stress peaks exceeding the bending strength. However, the results of low-cycle fatigue tests of atmospheric ice [9] show that no ice failure occurs due to cyclic load and fatigue during low-amplitude vibration.

5. Conclusion

This paper presents a finite element model which estimates the stresses developed in the ice cover of an overhead cable during aeolian vibration. In order to achieve this goal, first the aeolian vibration of an iced cable was simulated. The equations of cable motion during aeolian vibration were obtained from the basic equations of motion of a suspended cable and

a MATLAB code was developed to calculate the time histories of the cable motion, aerodynamic forces, additional horizontal tension acting in the cable during vibration, and torque due to springback. In the example considered in this study, a 10-cm-long piece of iced cable at mid-span was under examination, and the input data were determined at the two end points of that piece. A finite element model was constructed using the ABAQUS commercial software to calculate the stresses in the atmospheric ice accreted on the cable. The model showed that the highest stress along the vertical diameter of the ice occurred when the mid-point of the cable reached its highest and lowest positions. The maximum Von Mises stresses are 6210 Pa for the elements in the external layer, and 4056 Pa for the elements in the internal layer. These values are significantly less than the bending strength of atmospheric ice. According to this model, no ice failure occurs due to low-cycle fatigue and cyclic loads under the selected conditions of the atmospheric ice and cable during aeolian vibration. Using the method and the model developed in this study, the stress levels in atmospheric ice may be estimated for any other loading condition.

Acknowledgements

This work was carried out within the framework of the NSERC/Hydro-Quebec/UQAC Industrial Chair on Atmospheric Icing of Power Network Equipment (CIGELE) and the Canada Research Chair on Engineering of Power Network Atmospheric Icing (INGIVRE) at Université du Québec à Chicoutimi. The authors would like to thank the CIGELE partners (Hydro-Québec, Hydro One, Réseau Transport d'Électricité (RTE) and Électricité de France (EDF), Alcan Cable, K-Line Insulators, Tyco Electronics, CQRDA and FUQAC) whose financial support made this research possible.

References

[1] Abdel-Rohman, M., and Spencer, B. F., Control of Wind-Induced Nonlinear Oscillations in Suspended Cables, Nonlinear Dynamics 37 (2004) 341-355.

[2] Blevins, R. D., Flow induced vibration, Van Nostrand Reinhold, New York, 1990.

[3] CIGRE Working Group 01, Report on Aeolian Vibration, ELECTRA, NO. 124, 1978, pp. 21-77.

[4] CIGRE Working Group 11, Modelling of Aeolian vibration of single conductors: Assessment of the technology, ELECTRA, NO.181, 1998, pp. 53-69.

[5] EPRI, Transmission Line Reference Book: Wind-induced conductor motion, Electric Power Research Institute, Palo Alto, California, 1979.

[6] Irvine, H. M., and Caughey, T. K., The linear theory of free vibration of a suspended cable, Proc. R. Soc. Lond. A, 341 (1974) 299-315.

[7] Kermani, M., Farzaneh, M. and Gagnon, R. E., Bending Strength and Effective Modulus of Atmospheric Ice, Cold Regions Science and Technology, Vol. 53 (2008) 162-169.

[8] Fu, P., Modeling and simulation of the ice accretion process on fixed or rotating cylindrical objects by the boundary element method, Ph.D. thesis, University of Quebec at Chicoutimi, Chicoutimi, Quebec, 2004.

[9] Kermani, M., Farzaneh, M. and Kollár, L. E., Cyclic loads in power transmission lines and their effects on accreted atmospheric ice, IEEE Transactions on Power Delivery (2009) accepted.

[10] Luongo, A., and Piccardo, G., Non-linear galloping of sagged cables in 1:2 internal resonance, Journal of Sound and Vibration, 214(5) (1998) 915-940.

[11] Ohkuma, T., Kagami J., Nakauchi H., Kikuchi T., Takeda K., Marukawa H., Numerical Analysis of Overhead Transmission Line Galloping Considering Wind Turbulence, Electrical Engineering in Japan, 131(3) (2000) 1386-1397.

[12] Schwarz, J., Frederking, Gavrillov, R., Petrov, I.., Hirayama, K., Mellor, M., Tryde, P. and Vaudrey, K., Standardized testing methods for measuring mechanical properties of ice, Cold Regions Science and Technology, Vol. 4 (1981) 245-253.

[13] Van Dyke, P. and Havard, D. G., Effect of ice and snow on the dynamics of transmission line cables, Proc. 11th International Workshop on Atmospheric Icing of Structures, Montreal, Quebec, 2005.

Figure and table captions

Fig. 1. Cable displacement in horizontal, *U*, vertical, *V*, and transverse, *W*, directions.
Fig. 2. Loads and movement of a piece of cable on corresponding curves.
Fig. 3. The cable displacement in the middle of the span in vertical direction.
Fig. 4. Variation of distributed wind force in vertical direction.
Fig. 5. Variations of stresses due to additional dynamic tension in cable.
Fig. 6. Von Mises stresses in 4 elements in the external layer of atmospheric ice during aeolian vibration.
Fig. 7. Von Mises stresses in 4 elements in the internal layer of atmospheric ice during aeolian vibration.
Fig. 8. Position of the elements that are the subjects of Figs. 6, 7, 9 and 10.
Fig. 9. Normal stresses in 4 elements in the external layer of atmospheric ice.
Fig. 10. Normal stresses in 4 elements in the internal layer of atmospheric ice.
Fig. 11. Stress distribution along the horizontal diameter of cable-ice composition at 0.17s in aeolian vibration.
Fig. 12. Stress distribution along the vertical diameter of cable-ice composite at 0.17s in aeolian vibration.

Table 1. Characteristics of the span, cable and ice

Figures

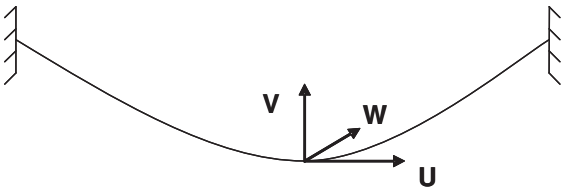

Fig. 1.

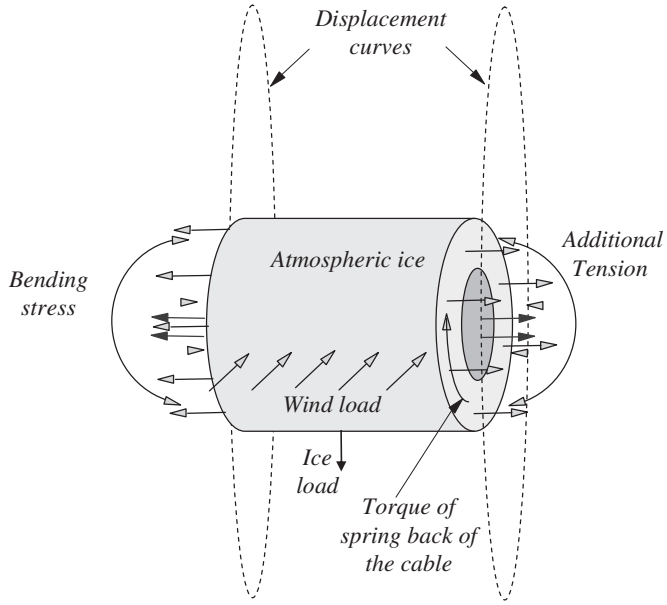
Displacement
curves
Bending
stress
Atmospheric ice
Additional
Tension
Wind load
Ice
load
Torque of
spring back of
the cable

Fig. 2.

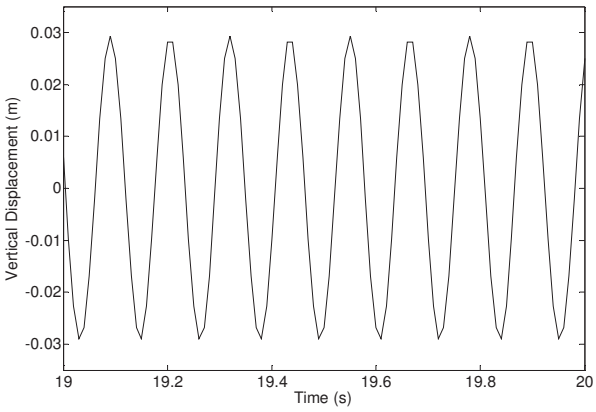
0.03
0.02
0.01
0
-0.01
-0.02
-0.03
Vertical Displacement (m)
19
19.2
19.4
19.6
19.8
20
Time (s)

Fig. 3.

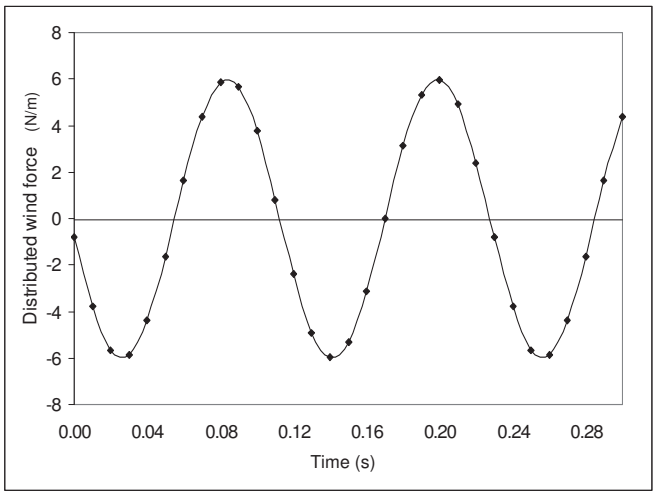
Distributed wind force (N/m)
8
6
4
2
0
-2
-4
-6
-8
0.00
0.04
0.08
0.12
0.16
0.20
0.24
0.28
Time (s)

Fig. 4.

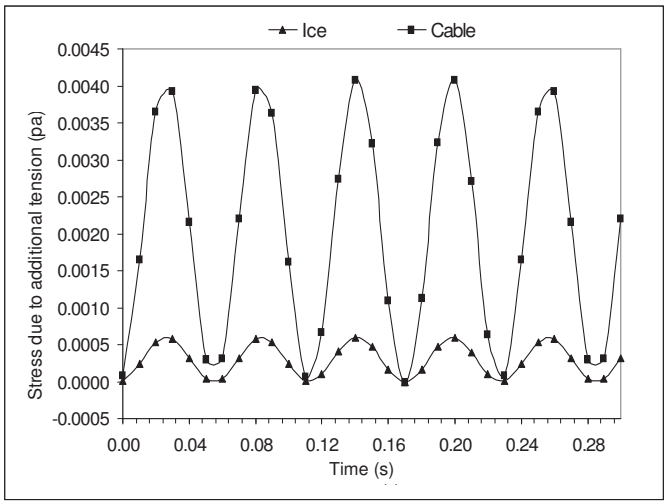
Ice
Cable
Stress due to additional tension (pa)
0.0045
0.0040
0.0035
0.0030
0.0025
0.0020
0.0015
0.0010
0.0005
0.0000
-0.0005
0.00
0.04
0.08
0.12
0.16
0.20
0.24
0.28
Time (s)

Fig. 5.

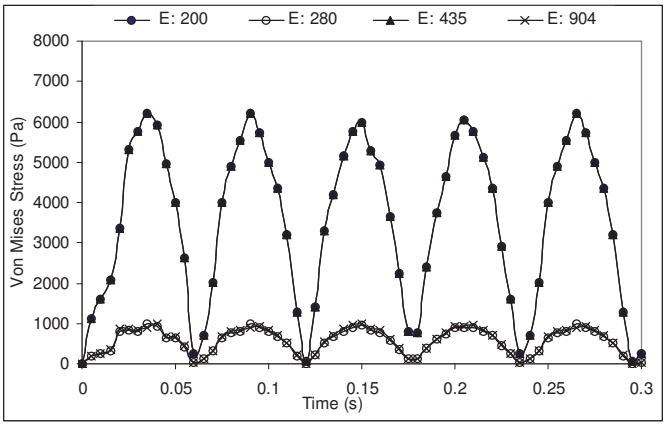
E: 200
E: 280
E: 435
E: 904
Von Mises Stress (Pa)
8000
7000
6000
5000
4000
3000
2000
1000
0
0
0.05
0.1
0.15
0.2
0.25
0.3
Time (s)

Fig. 6.

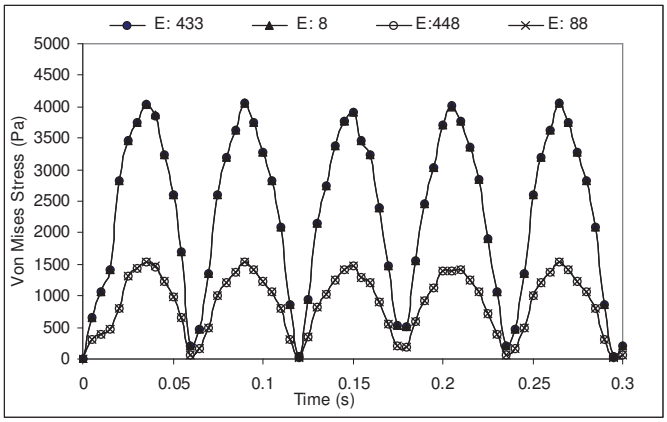
E: 433
E: 8
E:448
E: 88
Von Mises Stress (Pa)
5000
4500
4000
3500
3000
2500
2000
1500
1000
500
0
0
0.05
0.1
0.15
0.2
0.25
0.3
Time (s)

Fig. 7.

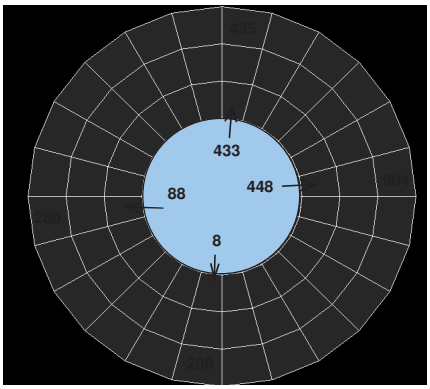

Fig. 8.

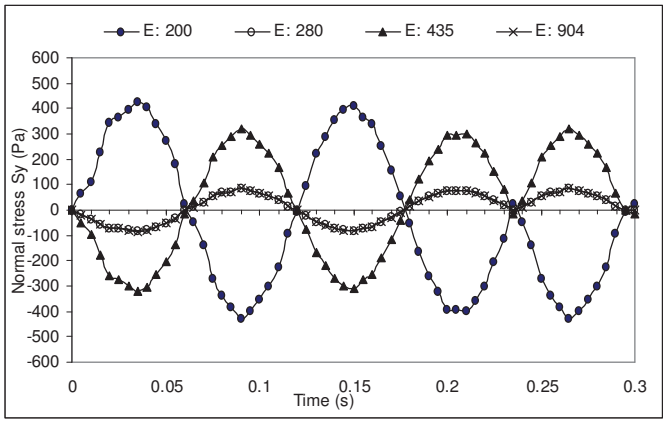
E: 200
E: 280
E: 435
E: 904
Normal stress Sy (Pa)
600
500
400
300
200
100
0
-100
-200
-300
-400
-500
-600
0
0.05
0.1
0.15
0.2
0.25
0.3
Time (s)

Fig. 9.

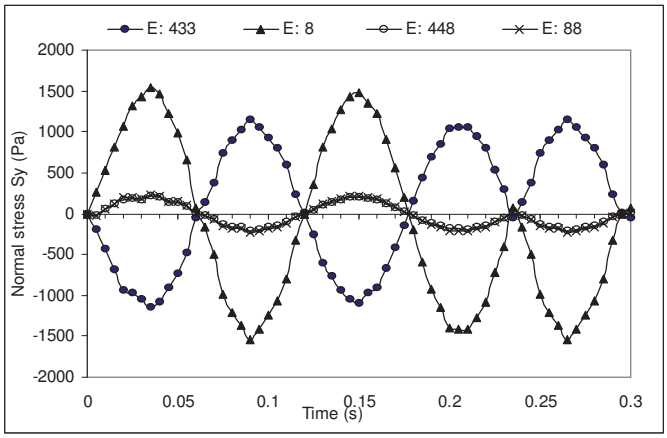
E: 433
E: 8
E: 448
E: 88
2000
1500
1000
500
0
-500
-1000
-1500
-2000
Normal stress Sy (Pa)
0
0.05
0.1
0.15
0.2
0.25
0.3
Time (s)

Fig. 10.

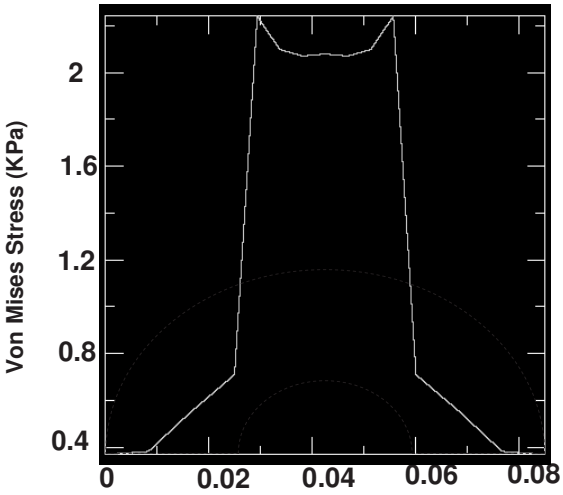

Fig. 11.

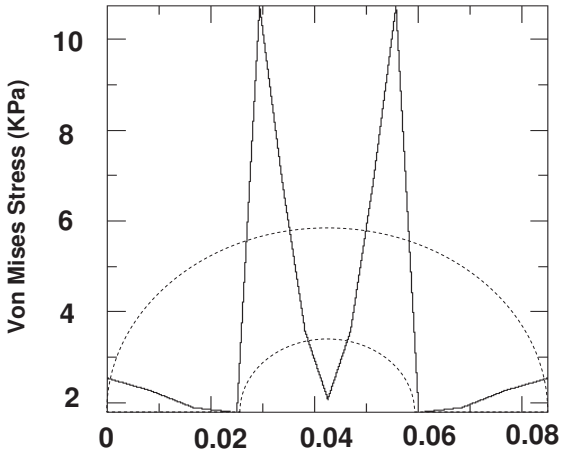

Fig. 12.

Tables

Parameter	Value	Unit
Cable type	BERSIMIS ACSR 42/7	---
Cable diameter	35.1	mm
Young's modulus of cable	62	GPa
Mass per unit length of cable	2.185	kg/m
Cable torsional rigidity	351	N.m/Rad
Cable cross-section area	725.2	mm^2
Span length	300	m
Cable sag	8.04	m
Ice type	Hard rime and glaze	---
Ice thickness on cable	25	mm
Density of ice	900	Kg/m^3
Young's modulus of ice	9	GPa
Wind velocity	4	m/s
Rotation angle due to ice accretion at span centre	405	Degree

Table 1